CRYSTAL GROWTH & DESIGN

pubs.acs.org/crystal

Article

Effect of Crystal Structure and Phase on the Dielectric, Ferroelectric, and Piezoelectric Properties of Ca^{2+}- and Zr^{4+}-Substituted Barium Titanate

Shahaji P. Kharat, Swati K. Gaikwad, Paul Gaurav Nalam, Rahul C. Kambale, Ajit R. James, Yesh D. Kolekar,* and C. V. Ramana*

Cite This: *Cryst. Growth Des.* 2022, 22, 5571−5581

Read Online

ACCESS | Metrics & More | Article Recommendations | Supporting Information

ABSTRACT: Barium titanate ($BaTiO_3$) and its associate ternary metal oxide systems constitute versatile materials with immense potential for various technological applications in electronics and optoelectronics. Herein, we report on the synthesis and property optimization of lead-free ceramic samples, namely $BaTiO_3$ (BT), $BaZr_{0.2}Ti_{0.8}O_3$ (BZT), $Ba_{0.7}Ca_{0.3}TiO_3$ (BCT), and $BaZr_{0.2}Ti_{0.8}O_3$−0.5 $Ba_{0.7}Ca_{0.3}TiO_3$ (BZT−BCT) composites. All of these materials were synthesized by the standard solid-state chemical reaction method, where tuning the composition and the crystal structure yields materials suitable for multifaceted applications related to capacitors, memory storage, and high-energy switching and transducers. Structural studies carried out using X-ray diffraction and Raman spectroscopy confirm the tetragonal phase for BT, BZT, and BZT−BCT samples, whereas BCT is a biphasic crystal system, which contains a small amount of the $CaTiO_3$ phase. Scanning electron microscopy characterization of the surface morphology indicates the granular-dense microstructures of all of the samples. Energy dispersive spectroscopy confirms the high degree of purity and chemical homogeneity of the synthesized samples in addition to a well-maintained composition. Density measurements using Archimedes principles show that all of the samples have densities above 4.96 g/cm^3. All of these materials exhibit typical polarization−electric field (P−E) hysteresis and field-induced strain butterfly (S−E) loops, which confirm their ferroelectric and piezoelectric nature. The frequency response of the dielectric constant shows a maximum dielectric constant of 2441 for pure BT and it decreases for higher frequencies, above 0.1 MHz. The dielectric properties of BT imply significant prospects for its future capacitor applications. Ferroelectric measurements, which are established by measuring the P−E hysteresis loop at 300 K, show that the BCT samples exhibit a 0.50 squareness ratio. The detailed analyses indicate that BCT is a candidate material for permanent memory storage device (FeRAM) applications, whereas BZT is good for switching applications. Furthermore, a moderately higher remnant polarization (P_r = 10.81 μC/cm^2) is obtained for BT and a lower coercive field (E_c = 0.78 kV/cm) is obtained for the BZT sample. Also, piezoelectric coefficient and strain measurements show that BT has a piezoelectric coefficient of 183 ± 1 pC/N and a converse piezoelectric coefficient of 365.7 ± 2 pm/V, which are the highest values. The Q-factor for the BZT−BCT composite was observed to be 4.16 × 10^{-4} (cm^2/μC)^2, which is maximum, implying that BZT−BCT is suitable for energy conversion transducer applications. In this work, we comprehensively elucidate and discuss the properties and potential applications of BT and its associated ternary metal oxide systems.

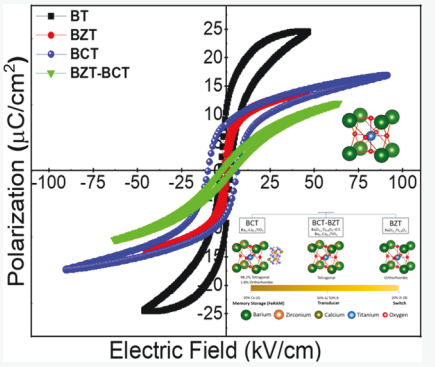

INTRODUCTION

In recent years, many countries have added new amendments to legislation and have imposed stringent restrictions on the use of lead (Pb) and Pb-based piezoelectric materials. These limitations started with Restrictions of Hazardous Substances (RoHS) directives imposed by the European Union (EU) to control the routine use of toxic materials in electrical and electronic devices such as capacitors, memory devices, sophisticated systems, electronic toys, etc. Before this regulation, the well-known PZT ($PbZr_{0.48}Ti_{0.52}O_3$) was extensively used.[1,2] Despite its superior properties compared to other piezoelectric materials, PZT is banned due to Pb toxicity; thus, it is required that the scientific and engineering research community develop Pb-free materials, which can exhibit properties comparable or even superior to PZT. However, in general, lead-free piezoelectric ceramics have inferior piezoelectricity (d_{33} < 150 pC/N in most cases), lower Curie temperature, and high dielectric loss as compared to PZT. Recently, their limit has been pushed to a higher level of piezoelectricity, d_{33} = 300−700 pC/N.[3,4] Liu and Ren reported

Received: June 17, 2022
Revised: July 19, 2022
Published: July 29, 2022

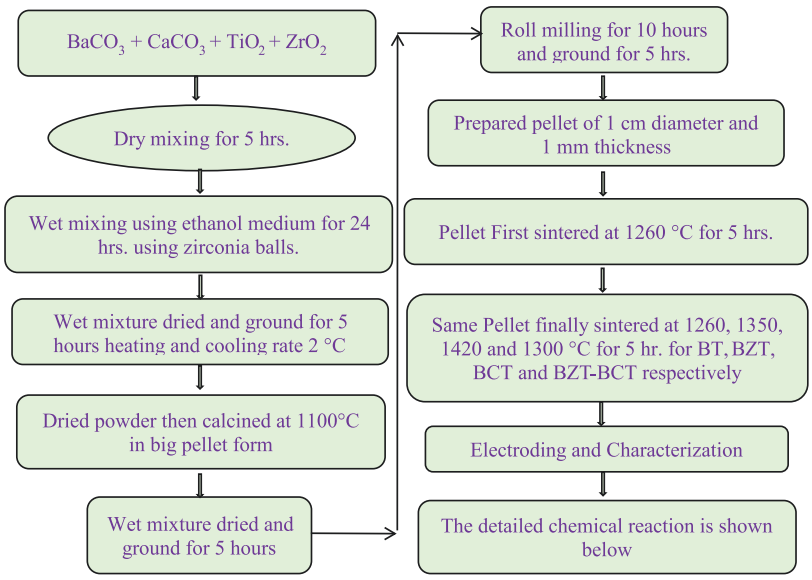

Figure 1. Flowchart explaining the synthesis of BZT−BCT using the solid-state reaction method.

the piezoelectric response ($d_{33} \sim 600$ pC/N) in (Ba, Ca)(Ti, Zr)O_3 (abbreviated as BZT−BCT) ceramics.[5] This system is fully Pb-free and environment-friendly and has thus attracted great attention.[6−10] The improved piezoelectric properties of BZT−BCT were due to the cubic−tetragonal−rhombohedral triple point.[5] Thus, BT, BZT, BCT, and BZT−BCT are interesting compounds, which may have the potential to replace PZT and other Pb-based materials. It is also reported that, despite the similarity of the phase diagrams of BZT−BCT and the substituted (Hf, Zr, or Sn) $BaTiO_3$ systems,[11−13] the piezoelectric response in Hf-, Zr-, and Sn-modified $BaTiO_3$ is considerably lower ($d_{33} \sim 300$−400 pC/N) than that of BZT−BCT ($d_{33} \sim 600$ pC/N).[5] Thus, restrictions all over the world have greatly incentivized the development of environment-friendly Pb-free materials, considering the toxicity of lead.[14−17] Therefore, in the fields of high-energy devices, capacitors, transducers, and switches, and electromechanical devices, the main focus of researchers in the last decade or two was to develop alternate forms of material systems to circumvent the use of lead. In this respect, $BaTiO_3$-based (Ba, Ca) (Ti, Zr)O_3, (Ba, Ca)(Ti, Sn)O_3, and (Ba, Ca) (Ti, Hf)O_3 compounds have established themselves as materials with great prospects.[18−21] These materials have evolved to the extent that their potential applications have spanned across numerous technologies, particularly in electronics, optoelectronics, energy storage and conversion device applications.[5,14−22]

The $BaTiO_3$-based compounds have a perovskite ABO_3 structure with space group *P4mm*, where *A* is a divalent cation (like Ba^{2+}, Ca^{2+}, etc.), which is at the corner of the unit cell, B is a tetravalent cation (like Ti^{4+}, Zr^{4+}, Sn^{4+}, Hf^{4+}, etc.) at the body center of the unit cell, and O^{2-} anions are at the face center.[20−22] The non-centrosymmetric nature of the central ions is a basis for the formation of permanent dipole moments in the perovskite structure.[22] Note that the scientific and engineering communities have been rigorously working to discover Pb-free alternative compounds with properties such as a high piezoelectric coefficient ($d_{33} \sim 600$ pC/N, compatible with PZT), higher spontaneous polarization, high remnant polarization ($P_r \geq 10$ μC/cm^2) and dielectric constant ($\varepsilon \geq 2000$ with low loss <0.001), and a transition temperature well above the room temperature. Liu et al. reported in 2009 that BZT−*x*BCT ($x = 0.5$) possesses a piezoelectric coefficient (d_{33}) of about 620 pC/N, a transition temperature of ∼100 °C, a dielectric constant of 3000 at room temperature, a saturation polarization of about 20 μC/cm^2, a remnant polarization of ∼15 μC/cm^2, a coercive field of ∼150 V/mm, a converse piezoelectric coefficient of ∼1150 pm/V, and maximum electro-strain.[5] All of these values are superior as compared to PZT, except the transition temperature. Due to this, it seems that BZT−*x*BCT ($x = 0.5$) can be a unique Pb-free composition that needs to be further explored. Many research groups have tried different compounds, changed the synthesis methods, and even attempted to tailor the microstructure for different applications, such as loud-speakers,[23,24] intravascular ultrasonic transducers,[18,23] energy storage devices,[25] sensors, actuators,[14,17] and capacitor applications.

Specifically, BZT−BCT is a pseudo-binary ferroelectric system with morphotropic phase boundary (MPB) composition.[5,26−29] Substitution of Zr^{4+} for Ti^{4+} enhances the dielectric constant,[27] and Ca^{2+} substitution for Ba^{2+} not only improves the dielectric constant ($\varepsilon = 1655$) with low loss ($\tan\delta = 0.013$) but also tailors the rise of Curie temperature.[25] Thus, the BZT−BCT composition accomplishes the basic requirement, as it has a high piezoelectric coefficient (d_{33}), high spontaneous polarization and dielectric constant, low loss (∼0.001), and a transition temperature well above the room temperature to facilitate the electric poling.

Practically, realizing superior ferroelectric and piezoelectric properties as compared to Pb-based materials is quite difficult. However, there is a possibility of some BT-based materials fulfilling the requirements of many applications, based on improved/modified ferroelectric and piezoelectric properties. For example, materials with a high dielectric constant with low loss are always desired for capacitive applications. A squareness ratio Mr/Ms close to 1 is required for permanent data storage applications. A high value of piezoelectric coefficients is required for piezosensor applications. Further, having a high value of the converse piezoelectric coefficient is good for electromechanical applications. But, so far, there is no single material/compound with superior properties as compared to Pb-based materials. Thus, in the present work, an attempt has been made to collectively look into the structural, dielectric,

https://doi.org/10.1021/acs.cgd.2c00679
Cryst. Growth Des. 2022, 22, 5571−5581

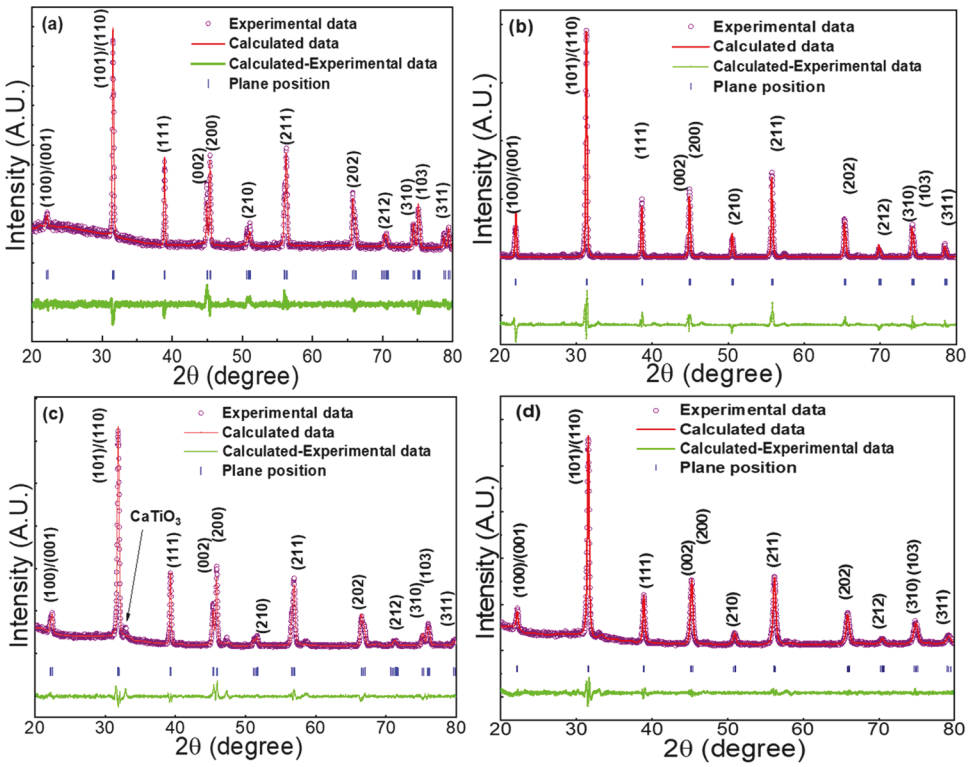

Figure 2. Rietveld fitted x-ray diffraction patterns of (a) $BaTiO_3$, (b) $BaZr_{0.2}Ti_{0.8}O_3$, (c) $Ba_{0.7}Ca_{0.3}TiO_3$, and (d) $BaZr_{0.2}Ti_{0.8}O_3$−0.5 $Ba_{0.7}Ca_{0.3}TiO_3$ samples.

ferroelectric, and piezoelectric properties, and to explore the suitable substituted barium titanate-based Pb-free ceramics for possible electronic device applications.

EXPERIMENTAL DETAILS

Synthesis. For the synthesis of BT, BZT, BCT, and BZT−BCT materials, AR grade raw chemicals were used in the standard ceramic method, so that there may be no ambiguity regarding the presence of any impurities. Thus, $BaCO_3$, $CaCO_3$, ZrO_2, and TiO_2 (all with purity 99.9%) were taken in stoichiometric proportion and weighed using a weighing balance with the least count of 1 microgram. Initially, all accurately weighed powders were ground for 5 h each and then were mixed using zirconia balls in a roll milling machine for 24 h, using ethanol as a mixing medium.[25] These turbid solutions were taken in a plate and zirconia balls were removed. The resulted solutions were heated at 82 °C in an oven to remove the ethanol. Then, the dried powders were ground in an agate mortar for 5 h. These powders were made into pellets using 1 ton per square inch pressure and heated in an alumina crucible. These pellets were heated at 1100 °C for 5 h with a heating and cooling rate of 2 °C/min as maintaining the heating and cooling rate is important for the reaction. Then, the pellets were removed and ground using agate mortar for 5 h and again roll milled for 10 h. The same procedure was repeated for different compounds. The detailed chemical reaction is shown below

$$(1-x)BaCO_3 + xCaCO_3 + (1-y)TiO_2 + yZrO_2 \xrightarrow{\text{(sintering)}} Ba_{1-x}Ca_xTiO_3 - 0.5BaZr_yTi_{1-y}O_3 + (x+y)CO_2 \quad (1)$$

The x and y values were varied as follows: for pure BT, $x = 0$ and $y = 0$; for BZT, $x = 0$ and $y = 0.2$; for BCT, $x = 0.3$ and $y = 0$; and for BZT−BCT, $x = 0.3$ and $y = 0.2$ mole percent. As an illustration, the detailed procedure for the BT−BCT is given below. The molar mass of one mole of each of the raw materials is taken as 197.34 g/mol for $BaCO_3$, 79.86 g/mol for TiO_2, 100.08 g/mol for $CaCO_3$, and 123.22 g/mol for ZrO_2. The specific reaction for BZT−BCT is as follows

$$0.7BaCO_3 + 0.3CaCO_3 + 0.8TiO_2 + 0.2ZrO_2 \xrightarrow{\text{(sintering at 1300 °C)}} Ba_{0.7}Ca_{0.3}TiO_3 - 0.5BaZr_{0.2}Ti_{0.8}O_3 + CO_2 \quad (2)$$

These raw materials were weighed (calculations are included in the Supporting Information) precisely and the following procedure was followed. The synthesis procedure for all materials is schematically presented in Figure 1.

All of the compounds were cylindrically pelletized (1 cm in diameter and 1 mm in thickness) and then sintered as BT at 1260 °C, BZT at 1350 °C, BCT at 1420 °C, and BZT−BCT at 1300 °C for densification of the pellets. First, all the four compounds were characterized using the X-ray diffraction pattern. Then, after electroding using silver paste, the pellets were used for different characterizations.

Characterization. Structural studies using X-ray diffraction (XRD) were done by employing the D8 Advance (Bruker Inc., Germany) instrument. Measurements were made using Cu Kα radiation, λ = 1.5406 Å. Some of the pellet samples were platinum coated for microstructural analysis using JEOL SEM. To remove the problem of space charge effect arising during the secondary electron detection, all of the samples were ground using a conducting carbon tape. Also, the atomic and weight percentage measurements were made using energy dispersive spectroscopy (EDS). The sintered cylindrical pellets of diameter 1 cm and thickness 1 mm were polished using sand paper, and conductive silver (Ag) paste was applied on both surfaces of the pellets for good electrical contacts. Then, these pellets were used for the dielectric measurements, which were made using a Hioki 3532−50 LCR meter in the range of 42 Hz to 5 MHz. Polarization versus electric field measurements (P vs E hysteresis loops) were performed using a Piezoelectric Evaluation System, TF analyzer 2000 from M/s aixACCT GmbH. Moreover, polarization versus electric field (P vs E) measurements were carried out using a triangular waveform at 1 Hz frequency. The density measurements of the samples were carried out using Archimedes principle with toluene solution. The Ag-pasted samples were electrically poled approximately

https://doi.org/10.1021/acs.cgd.2c00679
Cryst. Growth Des. 2022, 22, 5571−5581

Table I. Structural Parameters, Density, and Particle Size for All of the Samples

composition	lattice parameter c (Å)	lattice parameter a (Å)	c/a ratio	density (g/cm^3)	average crystallite size (nm)	volume (Å^3)	chi square (χ^2)	profile factor (Rp)	weighted profile factor (Rwp)	expected weighted profile factor (Re)	average grain size (μm)
BT	4.0325	3.9951	1.00936	5.22	31.5	64.360	1.81	37.3	23.2	17.4	3
BZT	4.0332	4.0401	0.99829	4.96	34.6	65.829	20.1	28.4	45.9	9.32	10
BCT	3.9974	3.9561	1.01043	6.06	23.8	62.561	2.48	24.1	19.2	12.2	5
BZT−BCT	4.0185	4.0053	1.00329	5.21	24.8	64.467	1.8	19.7	16.8	12.5	0.8

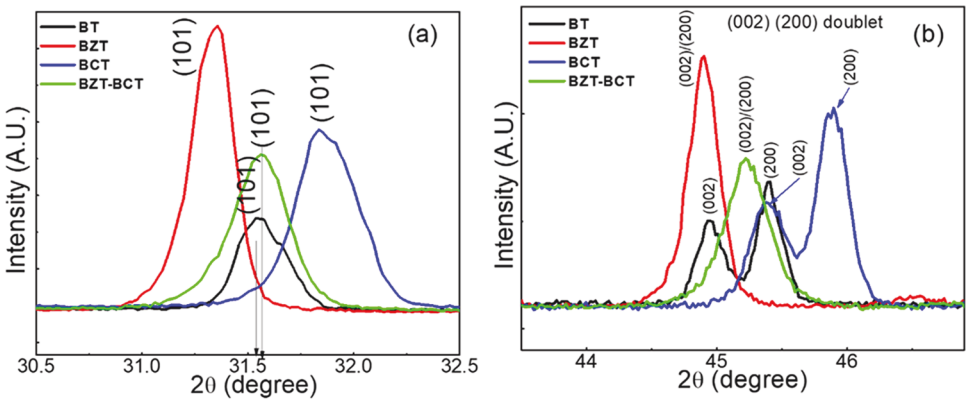

Figure 3. X-ray diffraction patterns of the (a) highest-intensity peak (101) of all ferroelectrics, and (b) doublet peaks confirming the tetragonal crystal structure.

at an electric field three times that of the coercive field ($E_{poling} = 3E_c$) for 30 min at 70 °C temperature. This poling field is sufficient for polarization switching and also avoids the dielectric breakdown of the samples due to over-poling.[22] After aging for 24 h, the electrically poled samples were used to determine the piezoelectric coefficients (d_{33}) using a Piezo-d_{33} meter with 250 mN force.

RESULTS AND DISCUSSION

Crystal Structure and Phase. The experimental XRD patterns along with the Rietveld refinement data of all of the compounds are shown in Figure 2. We found that the combined experimental and Rietveld refinement data are quite useful to understand the structure evolution with variable processing conditions and dopants in simple and complex oxides.[30,31] Therefore, we extended the approach to these BT-based materials. The analyses indicate that BT, BCT, and BZT−BCT possess ferroelectric tetragonal phase, whereas BZT shows orthorhombic phase. For the BCT sample, a small peak at $2\theta = 32.94°$ was observed, which corresponds to the $CaTiO_3$ phase. Thus, the BCT sample is biphasic (tetragonal $BaTiO_3$+ orthorhombic $CaTiO_3$). As BT, BZT, and BZT−BCT show a tetragonal crystal structure without any impurity phase/s, it confirms that Zr^{4+} is substituted for the Ti^{4+} site and for BCT, Ca^{2+} is substituted for the Ba^{2+} site. Furthermore, in the case of the BZT−BCT sample, both the phenomena, i.e., the substitution of Zr^{4+} for Ti^{4+} and Ca^{2+} for Ba^{2+}, are confirmed. However, for BCT, due to the solubility limit of Ca^{2+} (=0.23 mole %) at Ba^{2+}, an additional $CaTiO_3$ phase is formed. This is due to the fact that we have substituted Ca^{2+} above the solubility limit, i.e., 0.30 mole%.[25] The quantitative analyses indicate 98.2% tetragonal (BCT) and 1.8% orthorhombic ($CaTiO_3$) phases. The quantitative percentages of the tetragonal and the orthorhombic phases present in the BCT composition were calculated using the following equation

$$\text{phase composition}(\%) = \left[\left(\frac{\text{integrated area of the respective phase}}{\text{cumulative integrated area of the phases present}}\right) \times 100\right] \quad (3)$$

The lattice constant values are listed in Table I for all of the compositions. The average crystallite size, which is estimated using XRD data, was found to be 34.6 nm for BZT, while it was 24.8 nm for BZT−BCT. The c/a ratio is greater than 1 for BT, BCT, and BZT−BCT samples, confirming the tetragonal crystal structure. The c/a ratio for the BZT sample confirms the orthorhombic lattice. Density measurements indicate that the BCT compound has the highest density of 6.06 g/cm^2.

In order to probe the structural features of the BT compounds, the magnified regions of select XRD peaks were considered. Figure 3a shows a shift in the highest-intensity peaks observed for the synthesized ferroelectric samples. Comparing the peak shift with respect to the parent BT compound, the peak shifts towards the lower 2θ for BZT, which may be due to an increase in the interatomic distance with Zr^{4+} substitution for Ti^{4+}. The ionic radius of Zr^{4+} (0.72 Å) is larger than that of Ti^{4+} (0.605 Å), which increases the interplanar spacing of the crystal lattice. On the other hand, for BCT, the peak shift is towards the higher 2θ side, which may be due to the substitution by the smaller-ionic-radius cation Ca^{2+} (1.34 Å) for the larger Ba^{2+} (1.61 Å) in the perovskite structure. With decrease in the interatomic distance, the interplanar spacing also decreases and thus, there is a shift to a higher 2θ angle.[32] In the case of BZT−BCT compounds, a peak shift is observed toward a slightly higher 2θ angle as a net effect of the substitutions. This may be due to a higher mole percent concentration of Ca^{2+} ($x = 0.30$) as compared to a lower mole% concentration of Zr^{4+} ($y = 0.20$) in the BZT−BCT samples.

Figure 3b shows an apparent doublet at ($2\theta \approx 45°$) for both the BT and BCT samples. The first peak in the doublet

https://doi.org/10.1021/acs.cgd.2c00679
Cryst. Growth Des. 2022, 22, 5571−5581

corresponds to the diffraction from the (002) plane and the second peak corresponds to the (200) plane. The broadening of the peak is seen for BZT and BZT−BCT compounds. Furthermore, it is also observed that the doublet or tetragonality of BZT and BZT−BCT samples is not clear as compared to BT and BCT compounds. Having a doublet with intensity difference is a clear indication that these compounds may exhibit good piezoelectric, ferroelectric, and dielectric properties.

Chemical Bonding. Spectroscopic characterization, such as Raman scattering, provides direct information on the chemical bonding. Raman spectroscopic analyses are quite useful particularly to understand the chemical bonding changes (if any) in the host structure due to the incorporation of dopant ions.[33,34] Therefore, in the present work, we relied on Raman spectroscopic measurements to understand the chemical bonding and Zr- and/or Ca-doping-induced changes in the chemical bonding in BT-based ferroelectrics. Particularly, to support the XRD results and confirm the perovskite crystal structure of all of the ferroelectric samples, the room-temperature Raman spectra shown in Figure 4 are considered.

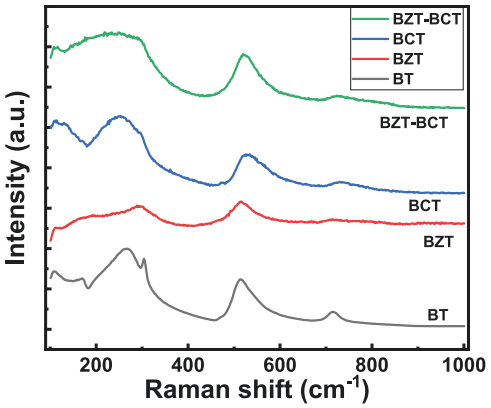

Figure 4. Raman spectra of BT-based compounds. The data shown are for $BaTiO_3$, $BaZr_{0.2}Ti_{0.8}O_3$, $Ba_{0.7}Ca_{0.3}TiO_3$, and $BaZr_{0.2}Ti_{0.8}O_3$−0.5 $Ba_{0.7}Ca_{0.3}TiO_3$ samples.

Raman active modes, peak positions, and reference peak positions are given in Table II. It is seen that the peaks corresponding to the octahedral sites formed by O^{2-} are visible and the intensity of the Raman active modes for BZT, BCT, and BZT−BCT decreased compared to pure BT. It is known that with the substitution of Ca^{2+} and Zr^{4+} for Ba^{2+} and Ti^{4+} in pure BT, there is a significant decrease in the intensity.[35] Predicting a possible reason for the intensity reduction is quite difficult as it involves Raman optical activity (ROA) theory, which contains many intensity-dependent tensor terms.[36,37] Therefore, the following logistic approach is considered. Ca and Ba are second-group elements and are from the fourth and sixth rows of the periodic table. As the Ca^{2+} substitutes for Ba^{2+}, the electron density decreases and thus the scattering intensity also decreases. Also, the radius of Ca^{2+} is smaller than that of Ba^{2+}, which further reduces the intensity. Also, if the same logic is used for Zr^{4+} substitution for Ti^{4+}, here Zr^{4+} has a larger radius but due to the shielding effect, the inner electrons do not take part in scattering and overall the intensity decreases.[36]

According to Raman tensor, the A(TO2) mode at 266.21 cm^{-1} has the maximum scattering efficiency.[36,37] Comparing Raman peaks with the reference data, it can be concluded that a pure phase is formed in all of the compounds, which corroborates the structural information obtained from XRD data. Because of the diffused peaks in the substituted ferroelectrics, the impurity peaks corresponding to the $CaTiO_3$ phase could not be detected through Raman spectra, while the signature is easily visible in the XRD patterns. The highest-intensity peak was observed close to 266.51 cm^{-1} for all of the ferroelectric samples. One additional peak was observed close to 110.16 cm^{-1}, which could not be associated with any of the reported Raman active modes.[26] Comparing the Raman spectra of the substituted samples with BT, it is evident that the peak at 304.16 cm^{-1} is absent for BZT, BCT, and BZT−BCT samples. According to earlier reports by Venkateswaran et al., the peak E(TO2 + LO1) at 304.16 cm^{-1} vanishes at high pressures above 3.6 GPa in BT.[38] Here, the strain generated due to the substitution of Ca^{2+} and Zr^{4+} might be responsible for the modification and vanishing of the peak corresponding to the E(TO2 + LO1) mode.[38,39]

Morphology and Microstructure. Surface morphology and topography, as revealed by the SEM micrographs shown in Figure 5, indicate that the BT microstructure is segregated broadly into two distinct grain sizes, small grains (1−2 μm) and large grains (5−8 μm). Small grains fit into the intergranular pores, which is essential to transfer the strain across the grain boundaries. The BZT sample has a maximum grain size of 10 μm, and therefore, the intergranular pores and grain boundaries are visible. For BCT, the BCT grains form a dense structure with interconnected grain boundaries. The BZT−BCT sample forms grains in the range of 0.8 μm, which are the smallest amongst all of the samples synthesized. Sintering temperature has a vital effect on the density and pore sizes in ferroelectric materials. The average grain size calculated from SEM and the densities of the samples measured using Archimedes principle are summarized in Table I. BCT samples tend to have the maximum density at 6.06 g/cm^3, whereas BZT samples have the least density at 4.96 g/cm^3. The density of BT and BZT−BCT is ∼5.21 g/cm^3. Note that the microstructure and density of the samples play an important role in properties such as dielectric constant, piezoelectric

Table II. Raman Modes and Peak Positions of the Ferroelectric Samples

modes	ref Raman mode (cm^{-1})	observed Raman mode (cm^{-1})			
		$BaTiO_3$	$BaZr_{0.2}Ti_{0.8}O_3$	$Ba_{0.7}Ca_{0.3}TiO_3$	$BaZr_{0.2}Ti_{0.8}O_3$-0.5$Ba_{0.7}Ca_{0.3}TiO_3$
		110.16	111.16	110.37	108.42
Al (TOl)	153	169.23			
Al (TO2)	259	266.51	294.04	295.16	292.73
E (TO2 + LOl)	306	304.16			
Al (TO3)	521	512.08	516.26	534.60	519.80
Al (LO3)	715	715.78			

https://doi.org/10.1021/acs.cgd.2c00679
Cryst. Growth Des. 2022, 22, 5571−5581

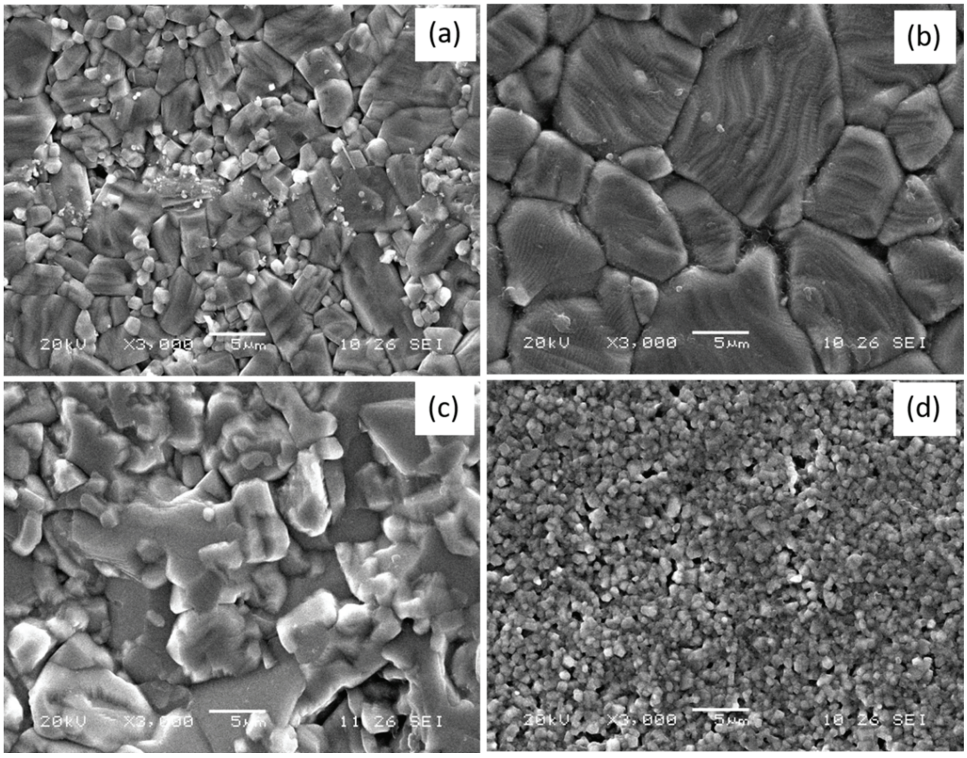

Figure 5. SEM images of (a) $BaTiO_3$, (b) $BaZr_{0.2}Ti_{0.8}O_3$, (c) $Ba_{0.7}Ca_{0.3}TiO_3$, and (d) $BaZr_{0.2}Ti_{0.8}O_3$−0.5 $Ba_{0.7}Ca_{0.3}TiO_3$ samples.

constant, and polarization−electric field (PE) behavior.[40] Figure S1 (supporting information) shows the EDS data of all of the samples. All of the samples show the presence of compositional elements (Table ST1). The EDS spectra and quantification analyses confirm and validate the chemical composition and chemical homogeneity of all of the samples synthesized.

Dielectric Properties. The frequency responses of the dielectric constants (Table III) for these materials are shown in Figure 6. The BT sample has the highest value of dielectric constant (ε' = 2441) at a frequency of 42 Hz, whereas the BCT sample has the lowest value of dielectric constant (ε' = 609) at a frequency of 42 Hz. A significant drop (Table III) in the dielectric constant for all of the samples is observed for applied frequencies above 0.1 MHz. There is only a 21.51% drop in the dielectric constant for the BCT sample compared to 97.80% drop for the BZT sample. Thus, BCT can retain a permanent dipole moment even up to the frequency of 1 MHz. The real part of the dielectric constant was calculated using the following relation[41,42]

$$\varepsilon' = \frac{1129 \times C(\mathrm{nF}) \times t(\mathrm{mm})}{A(\mathrm{cm}^2)} \quad (4)$$

Table III. Dielectric Constants of All Ferroelectric Samples

composition	maximum value of dielectric constant (at 42 Hz)	dielectric constant at high frequency (at 5 MHz)	% drop in dielectric constant
$BaTiO_3$	2441	398	83.69
$BaZr_{0.2}Ti_{0.8}O_3$	1095	24	97.80
$Ba_{0.7}Ca_{0.3}TiO_3$	609	478	21.51
$BaZr_{0.2}Ti_{0.8}O_3$−0.5 $Ba_{0.7}Ca_{0.3}TiO_3$	1768	529	70.07

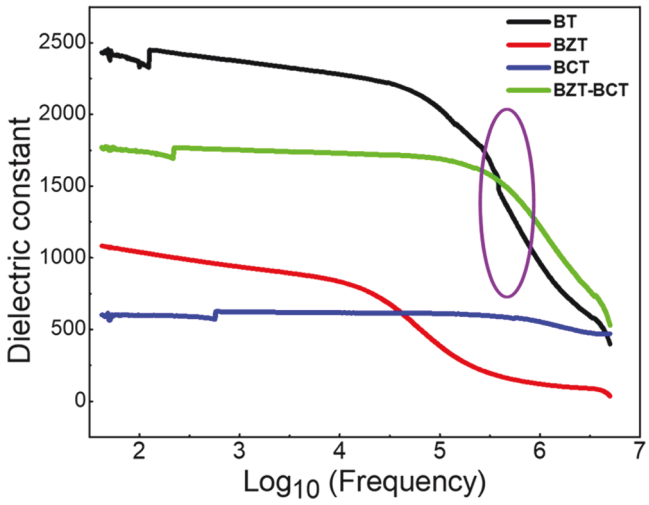

Figure 6. Variation of dielectric constant with frequency of all BT-based ferroelectrics. The data shown are for $BaTiO_3$, $BaZr_{0.2}Ti_{0.8}O_3$, $Ba_{0.7}Ca_{0.3}TiO_3$, and $BaZr_{0.2}Ti_{0.8}O_3$−0.5 $Ba_{0.7}Ca_{0.3}TiO_3$ samples.

where ε' is the real part of the dielectric constant, C is the capacitance of the materials in nano-Farad, t is the thickness of the sample in mm, and A is the area of the sample. The dielectric constant of a material is a cumulative effect of the permanent dipole moment, space charge polarization, and atomic and electronic polarizabilities.

The intensities of these parameters decrease as the frequency increases.[43] Dielectric measurements suggest that BT is the most suitable material for capacitor applications as it has a higher value of dielectric constant in the frequency range 42 Hz−5 MHz. In particular, the BZT−BCT sample sustains a dielectric constant for a slightly high-frequency range (0.38−5 MHz) as compared to all of the other synthesized compounds.

https://doi.org/10.1021/acs.cgd.2c00679
Cryst. Growth Des. 2022, 22, 5571−5581

Thus, BZT−BCT is suitable as a capacitive material for applications where the operating frequency range is higher (0.38−5 MHz), and the BCT sample can be used where a low dielectric constant ($\varepsilon \sim 500$) is acceptable, with a dielectric constant drop of just 21.5% at a higher frequency (5 MHz). According to Landolt−Brönstein series, it was expected to rise the dielectric constant for the Zr^{4+} (=0.020 mole %) substitution at Ti^{4+} in BT.[44]

The observed drop in the maximum value of dielectric constant for BZT is 56% compared to pure BT. This suggests that the dielectric constant is not only composition dependent but also depends on other parameters, particularly density. BZT has a lower density (4.96 g/cm^3) compared to the density of pure BT (5.22 g/cm^3). If we use a similar analogy for BCT, we expect a much higher value of dielectric constant as compared to pure BT. However, this is not the case as BCT has the presence of an impurity phase, $CaTiO_3$, due to the solubility limit (=0.25 mole %) of Ca^{2+} at the Ba^{2+} site in $BaTiO_3$.[25,45]

Ferroelectric Properties. To predict the usefulness of these materials in data storage applications, ferroelectric measurements were carried out. The PE measurements shown in Figure 7 confirm the ferroelectric nature of all of the samples.

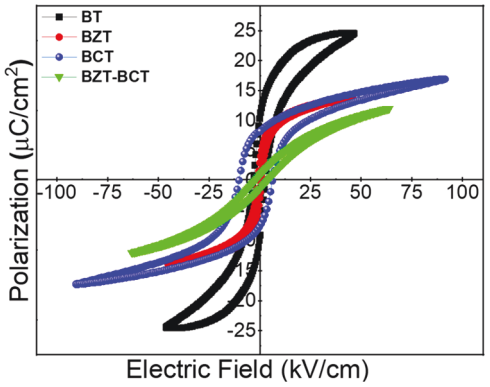

Figure 7. Electric polarization (P) versus applied electric field (E), i.e., $P-E$ hysteresis loops of all BT-based ferroelectrics. The data shown are for $BaTiO_3$, $BaZr_{0.2}Ti_{0.8}O_3$, $Ba_{0.7}Ca_{0.3}TiO_3$, and $BaZr_{0.2}Ti_{0.8}O_3$−0.5 $Ba_{0.7}Ca_{0.3}TiO_3$ samples.

Ferroelectric parameters for all of the samples are presented in Table IV. It is seen that the pure BT sample has a higher value of remnant polarization of 10. 81 μC/cm^2, which is essential for retaining stored data for a long time. The squareness ratio of the BCT sample is higher (squareness ratio, P_r/P_s = 0.5), and a higher value of coercivity (H_c = 6.41 kV/cm) is good for permanent memory device applications. The coercive electric field (H_c) should be small enough for less energy consumption (area enclosed by the PE loop) while writing the data, and it should be high enough so that the written data is not altered by exposing the ferroelectric materials to a lower electric field.[46,47] BZT and BZT−BCT samples have low coercivity, which may be suitable for volatile or random-access memory applications. A careful observation of the PE loop confirms that with Zr^{4+} substitution for Ti^{4+}, the coercivity decreased and with Ca^{2+} substitution for Ba^{2+}, the coercivity value is increased. Also, the BZT−BCT sample has a coercivity intermediate of BZT and BCT. Thus, the observed results suggest that if coercivity to be decreased, then Zr^{4+} can be substituted for Ti^{4+}, and if coercivity to be increased, then Ca^{2+} is to be substituted for Ba^{2+} within solubility limits.[48]

Current Density ($J-E$) Plots. The surface current density (J in μA/cm^2) measurements with an applied electric field for all samples are shown in Figure 8. The maximum value of

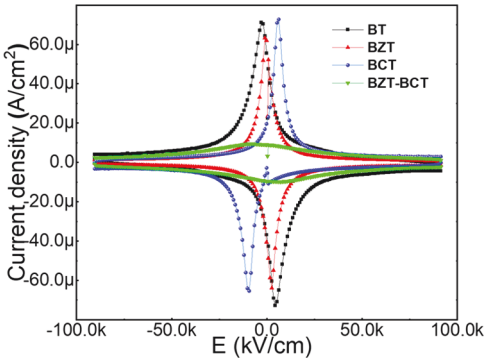

Figure 8. Current density (J) versus electric field of all BT-based ferroelectrics. The data shown are for $BaTiO_3$, $BaZr_{0.2}Ti_{0.8}O_3$, $Ba_{0.7}Ca_{0.3}TiO_3$, and $BaZr_{0.2}Ti_{0.8}O_3$−0.5 $Ba_{0.7}Ca_{0.3}TiO_3$ samples.

current density for all ferroelectric samples is given in Table IV. The BT, BZT, and BCT samples show sharp peaks, which indicates that the sample is fully saturated,[49] and the same is also confirmed from the PE loops. For the BCT sample, the highest value of surface current obtained is 72.1 μA/cm^2, which drops down to 9.33 μA/cm^2 for the BZT−BCT sample. BZT−BCT doesn't have a sharp peak, which is an indication that the sample is not fully saturated. The values of remnant polarization and saturation polarization are observed to decrease compared to the reported values.[7,28,50] The $J-E$ measurements indicate that, with substitution of Zr^{4+} and Ca^{2+} for Ti^{4+} and Ba^{2+}, the polarization becomes slow and the ferroelectric domain orientation becomes slower as compared to the parent compound BT.

Strain ($S-E$) Plots. Figure 9 shows the electric strain as a function of the applied electric field. Due to the application of an external voltage, the material gets strained, which changes the dimensions of the materials, and the strain is given by the equation[51]

$$(S_3 = d_{33}^* \times E_3) \tag{5}$$

where S_3 is the maximum strain along the Z-axis along which the electric field is applied, d_{33}^* denotes the converse

Table IV. Ferroelectric Parameters and Current Density for All Ferroelectric Samples

composition	p_{max} (μC/cm^2)	P_r (uC/cm^2)	E_c (KV/cm)	E_{max} (KV/cm)	squareness ratio	J (μA/cm^2) (max)
BT	24.20	10.81	3.02	46.59	0.446	70.4
BZT	13.82	3.24	0.78	45.64	0.234	62.1
BCT	16.86	8.44	6.41	90.78	0.500	72.1
BZT−BCT	12.00	1.19	1.92	63.74	0.099	9.33

https://doi.org/10.1021/acs.cgd.2c00679
Cryst. Growth Des. 2022, 22, 5571−5581

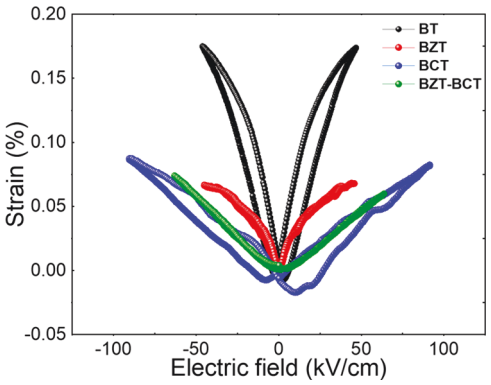

Figure 9. Strain versus applied electric field for all of the BT samples.

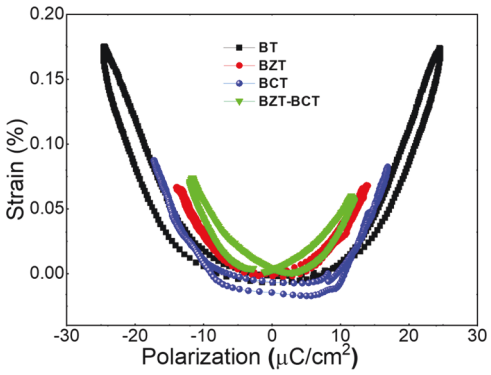

Figure 10. Strain versus electric polarization of BT-based compounds.

piezoelectric coefficient (if the field is applied along the Z-axis and change in dimensions is measured along the Z-axis), and E_3 is the maximum applied electric field.

Apparent converse piezoelectric coefficients calculated for all of the samples are shown in Table V. The shape of the polarization loop for BT and BCT is prominently due to polarization switching and domain walls' motion. The BT sample has a maximum value of strain, which is ∼0.174%, and BZT−BCT has the least value of strain of 0.06%. The BT sample has the highest value of converse piezoelectric coefficient of 365.7±2 pm/V. The high value of strain for BT may be due to the easy motion of the ferroelectric domain.[52] If a comparison is made among the other three substituted samples, BZT has a higher value of d_{33}^* (147.7 ± 2 pm/V) for both the positive and negative electric cycles. With Zr^{4+} substitution, the gap of the loop decreases for both the BZT and BZT−BCT samples. For the BCT sample, a drastic change in strain is observed around 60 kV/cm. For BT and BZT−BCT samples, the strain varies smoothly, which is useful for electromechanical transducer applications.[18] All of the samples have a symmetric nature of S−E loops, which is one of the prerequisites for AC applications.[50] Furthermore, for the BT sample, the value of strain is 0.174% and is comparable to lead-based ferroelectric materials.[53]

Electrostriction Study. Figure 10 shows the electrostriction measurements for all of the ferroelectric samples. The Q-factor can be calculated from these graphs using the formula[54]

$$Q = \frac{S}{P^2} \tag{6}$$

where Q is the electrostrictive coefficient, S is the strain, and P is polarization. The electrostrictive coefficient for the BZT−BCT sample is observed to be 4.16×10^{-4} $(cm^2/\mu C)^2$, which is the highest among all of the ferroelectric samples under study. This suggests that the BZT−BCT sample may be more suitable for electromechanical actuator applications.[17,26,55] The Q-factors for all of the ferroelectric samples are presented in Table VI.

The comparison of piezoelectric coefficient (d_{33}) values measured for the materials in the present study and for the materials in the literature are tabulated in Table VII.

Piezoelectric Properties. The piezoelectric coefficients (d_{33}) measured for all of the BT-based samples are tabulated in Table VI. BT has a maximum value of piezoelectric coefficient of 180 pC/N, whereas BZT exhibits the minimum of 44 pC/N. Among the substituted compounds, BCT has a maximum piezoelectric coefficient value, 122 pC/N. Overall, there is a decrease in piezoelectric coefficient values for all of the substituted samples as compared to the parent compound BT. From the converse piezoelectric coefficient (d_{33}^*) values (see Table V), it is seen that even if the d_{33}^* value for BCT is lower (90.9 pm/N along the positive side and −98.9 pm/N along the negative side), the value of piezoelectric coefficient (d_{33} = 122 pC/N) is much higher as compared to other cation-substituted compounds. This means that BCT is more suitable for applications where the direct piezoelectric coefficient is applicable and BZT is suitable for applications where a high value of the converse piezoelectric coefficient is required. Furthermore, piezoelectric coefficient values are higher for samples that are 3 μm (BT) to 5 μm (BCT) in size. If the size is less (0.8 μm for BZT−BCT) or more (10 μm for BZT), then the piezoelectric coefficient values are observed to decrease. Thus, a ferroelectric sample having the optimum microstructure along with a higher density plays a vital role in determining the piezoelectric coefficients.[63] Based on the comprehensive and detailed comparative study performed, we present the summary of the findings and implications schematically in Figure 11. The schematic diagram (Figure 11) describes the various lattice structures that emerge when BT is doped with Ca and Zi, and their respective or possible applications based on the properties studied.

SUMMARY AND CONCLUSIONS

Intrinsic and Zr-, Ca-substituted $BaTiO_3$ (BT, BZT, and BCT) and BZT−BCT composite samples were successfully synthesized by the high-temperature solid-state chemical reaction method. The structural characterization of all of the BT, BZT,

Table V. Converse Piezoelectric Constants for All Ferroelectric Samples

composition	strain (%)	electric field (kV/cm)	+ve d_{33}* (pm/V)	strain (%)	electric field (kV/cm)	−ve d_{33}* (pm/V)
$BaTiO_3$	0.1741	47.60	365.7	−47.51	0.1748	−367.9
$BaZr_{0.2}Ti_{0.8}O_3$	0.0687	46.51	147.7	−45.27	0.0666	−147.1
$Ba_{0.7}Ca_{0.3}TiO_3$	0.0838	92.11	90.9	−89.78	0.0888	−98.9
$BaZr_{0.2}Ti_{0.8}O_3$−0.5 $Ba_{0.7}Ca_{0.3}TiO_3$	0.0608	66.52	91.4	−64.19	0.759	−118.2

https://doi.org/10.1021/acs.cgd.2c00679
Cryst. Growth Des. 2022, 22, 5571−5581

Table VI. Piezoelectric Parameters for all BT-based Ferroelectric Samples

composition	P_{max} (μC/cm^2)	$(P_{max})^2$ (μC/cm^2)^2	% strain (max)	Q (=S/P^2) (cm^2/μC)^2	d_{33} (pC/N)	maximum applied electric field for poling (kV/cm)
BT	21.41	458.388	0.170	3.71×10^{-4}	180	9.06
BZT	14.23	202.493	0.071	3.51×10^{-4}	44	2.34
BCT	16.94	286.964	0.083	2.89×10^{-4}	122	13
BZT−BCT	11.81	139.476	0.058	4.16×10^{-4}	61	5.76

Table VII. Piezoelectric Coefficient Values of the Four Samples and Materials in the Literature[a]

composition	piezoelectric coefficient (d_{33}) (pC/N)
BT	180
BZT	44
BCT	122
BZT−BCT	61
Mo/Cr-doped $CaBi_2Nb_2O_9$[56]	15
$LiSbO_3$-$(Na_{0.5}K_{0.5})NbO_3$[56]	143
BNLKT4-28[57]	135
BNT-0.3[58]	92
BZT-Portland cement[59]	10
BCT[6060]	130
BZT−BCT (thin films)[5,61]	620
BT-based systems[62]	150

[a]The reference number is indicated as a superscript to the material name.

BCT, and BZT−BCT samples confirms the tetragonal structure of the BT, BCT, and BZT−BCT samples. However, BZT crystallizes in orthorhombic structure, while formation of the additional phase, $CaTiO_3$, occurs for BCT. The average crystallite size was maximum (34.6 nm) for BZT. SEM analyses also indicate grain growth for the BZT sample and a dense microstructure for BCT. The physical density and measured piezoelectric coefficient (d_{33}) values are in direct correlation with each other, suggesting that the piezoelectric variability in BT, BZT, BCT, and BZT−BCT is primarily due to their corresponding crystal structure and density. The P−E loops suggest that when coercivity to be decreased, Zr^{4+} can be substituted for Ti^{4+}, and if coercivity is to be increased, then Ca^{2+} is to be substituted for the Ba^{2+} site. The squareness ratio (P_r/P_s) of the BCT sample is higher ($P_r/P_s = 0.5$), and a higher value of coercivity (E_c = 6.41 kV/cm) is good for permanent memory device applications. The J−E plots indicate the enhanced ability of BCT to hold the maximum electric field with the highest value of surface current, 72.1 μA/cm^2. For both the BT and BZT−BCT samples, the strain varies smoothly, which is useful for electromechanical transducer applications. BZT−BCT exhibits the highest Q-factor (4.16×10^{-4} (cm^2/μC)^2), which is more suitable for electromechanical applications. Thus, by studying comparatively, we conclude that BT-based materials are useful for a variety of electronic device applications; however, the doping and relative structural and physical properties must be optimized to derive enhanced properties and performance.

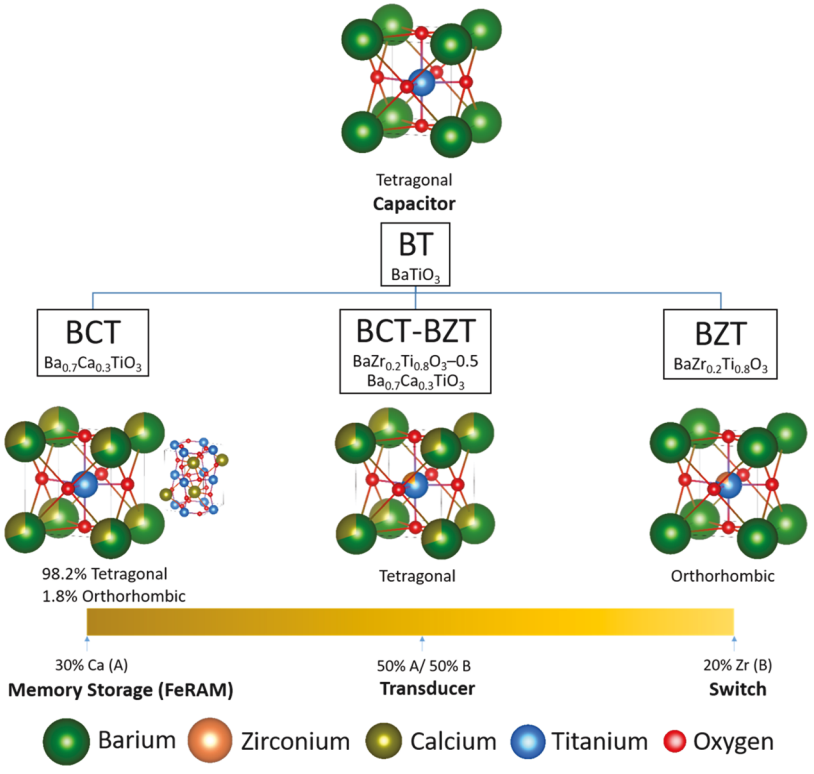

Figure 11. Schematic diagram showing various crystal systems of intrinsic and substituted $BaTiO_3$. The different phases and crystal systems make BT and its associate ternary metal oxide systems versatile materials for a plethora of applications.

https://doi.org/10.1021/acs.cgd.2c00679
Cryst. Growth Des. 2022, 22, 5571−5581

■ ASSOCIATED CONTENT

Supporting Information

The Supporting Information is available free of charge at https://pubs.acs.org/doi/10.1021/acs.cgd.2c00679.

Additional details of mass/weight calculations for the synthesis, EDS data and composition estimation of all the BT-based compounds are included in the Supporting Information (PDF)

■ AUTHOR INFORMATION

Corresponding Authors

Yesh D. Kolekar − *Department of Physics, Savitribai Phule Pune University, Pune 411007 Maharashtra, India;* orcid.org/0000-0002-9466-3184; Email: ydkolekar@gmail.com

C. V. Ramana − *Centre for Advanced Materials Research (CMR), University of Texas at El Paso, El Paso, Texas 79968, United States; Department of Mechanical Engineering, University of Texas at El Paso, El Paso, Texas 79968, United States;* orcid.org/0000-0002-5286-3065; Email: rvchintalapalle@utep.edu

Authors

Shahaji P. Kharat − *Department of Physics, Savitribai Phule Pune University, Pune 411007 Maharashtra, India; Department of Physics, Fergusson College (Autonomous), Pune 411004 Maharashtra, India*

Swati K. Gaikwad − *Department of Physics, Savitribai Phule Pune University, Pune 411007 Maharashtra, India; Department of Physics, Fergusson College (Autonomous), Pune 411004 Maharashtra, India*

Paul Gaurav Nalam − *Centre for Advanced Materials Research (CMR), University of Texas at El Paso, El Paso, Texas 79968, United States*

Rahul C. Kambale − *Department of Physics, Savitribai Phule Pune University, Pune 411007 Maharashtra, India*

Ajit R. James − *Ceramics and Composites Group, Defence Metallurgical Research Laboratory, (Ministry of Defence), Hyderabad, Telangana 500058, India*

Complete contact information is available at: https://pubs.acs.org/10.1021/acs.cgd.2c00679

Notes

The authors declare no competing financial interest.

■ ACKNOWLEDGMENTS

The authors are thankful to the Department of Science and Technology (Government of India), New Delhi for providing financial assistance (ref SR/FTP/PS-040/2010) to carry out the research work. S.P.K. and S.K.G. acknowledge the financial assistance from University Grant Commission for Basic Scientific Research (UGC-BSR) fellowships. The authors at the University of Texas at El Paso acknowledge, with pleasure, support from the National Science Foundation (NSF) with NSF-PREM grant #DMR-1827745.

■ REFERENCES

(1) Bernard, J.; William, R. C., JR.; Hans, J. Piezoelectric Ceramics. *J. Am. Ceram. Soc.* **1971**, 135−183.

(2) Uchino, K. Chapter 7. *Ferroelectric Devices*, CRC Press, 2010; Chapter 7, pp 1−85.

(3) Saito, Y.; Takao, H.; Tani, T.; Nonoyama, T.; Takatori, K.; Homma, T.; Nagaya, T.; Nakamura, M. Lead-free piezoceramics. *Nature* **2004**, *432*, 84−87.

(4) Zhao, C.; Wu, H.; Li, F.; Cai, Y.; Zhang, Y.; Song, D.; Wu, J.; Lyu, X.; Yin, J.; Xiao, D.; Zhu, J.; Pennycook, S. J. Practical High Piezoelectricity in Barium Titanate Ceramics Utilizing Multiphase Convergence with Broad Structural Flexibility. *J. Am. Chem. Soc.* **2018**, *140*, 15252−15260.

(5) Liu, W.; Ren, X. Large piezoelectric effect in Pb-free ceramics. *Phys. Rev. Lett.* **2009**, *103*, No. 257602.

(6) Tian, Y.; Chao, X.; Jin, L.; Wei, L.; Liang, P.; Yang, Z. Polymorphic structure evolution and large piezoelectric response of lead-free (Ba,Ca)(Zr,Ti)O_3 ceramics. *Appl. Phys. Lett.* **2014**, *104*, 112901.

(7) Yan-Qiang, L. A Short-wave UV Nonlinear Optical Sulfate of High Thermal Stability. *Chin. J. Struct. Chem.* **2020**, *305*, 116−123.

(8) Kun, C.; Shuai-Shuai, H.; Shu-Juan, H.; Tudi, A.; Zhi-ua, Y.; Shi-Lie, P. A New Double Alkali Metal Borate $LiRbB_8O_{13}$ with Large Bandgap and Birefringence. *Chin. J. Struct. Chem.* **2020**, *39*, 1578−1584.

(9) Pan, F. Can Structural Chemistry Point the Way: Exploring the Relevance between Structure and Properties. *Chin. J. Struct. Chem.* **2020**, *303*, 12.

(10) Fang-Yuan, C.; Jae-Ha, M.; Kui, X. Porous Iron Single Crystals at 2 cm Scale Delivering Enhanced Electrocatalysis Performance. *Chin. J. Struct. Chem.* **2020**, *39*, 2033−2040.

(11) Jonker, G. H.; Kwestroo, W. The Ternary Systems BaO-TiO_2-SnO_2 and BaO-TiO_2-ZrO_2. *J. Am. Ceram. Soc.* **1958**, *41*, 390−394.

(12) Yu, Z.; Ang, C.; Guo, R.; Bhalla, A. S. Piezoelectric and strain properties of Ba($Ti_{1-x}Zr_x$)O_3 ceramics. *J. Appl. Phys.* **2002**, *92*, 1489−1493.

(13) Yasuda, N.; Ohwa, H.; Asano, S. Dielectric Properties and Phase Transitions of Ba($Ti_{1-x}Sn_x$)O_3 Solid Solution. *Jpn. J. Appl. Phys.* **1996**, *35*, 5099−5103.

(14) Fu, J.; Hou, Y.; Zheng, M.; Zhu, M. Topochemical Conversion of (111) $BaTiO_3$ Piezoelectric Microplatelets Using $Ba_6Ti_{17}O_{40}$ as the Precursor. *Cryst. Growth Des.* **2019**, *19*, 1198−1205.

(15) Maxim, F.; Ferreira, P.; Vilarinho, P. M.; Aimable, A.; Bowen, P. Additive-Assisted Aqueous Synthesis of $BaTiO_3$ Nanopowders. *Cryst. Growth Des.* **2010**, *10*, 3996−4004.

(16) Panda, P. K. Review: environmental friendly lead-free piezoelectric materials. *J. Mater. Sci.* **2009**, *44*, 5049−5062.

(17) Rödel, J.; Jo, W.; Seifert, K. T. P.; Anton, E.-M.; Granzow, T.; Damjanovic, D. Perspective on the Development of Lead-free Piezoceramics. *J. Am. Ceram. Soc.* **2009**, *92*, 1153−1177.

(18) Acosta, M.; Novak, N.; Rojas, V.; Patel, S.; Vaish, R.; Koruza, J.; Rossetti, G. A.; Rödel, J. $BaTiO_3$-based piezoelectrics: Fundamentals, current status, and perspectives. *Appl. Phys. Rev.* **2017**, *4*, 041305.

(19) Yang, T.; Ke, X.; Wang, Y. Mechanisms Responsible for the Large Piezoelectricity at the Tetragonal-Orthorhombic Phase Boundary of (1-x)$BaZr_{0.2}Ti_{0.8}O_3$-x$Ba_{0.7}Ca_{0.3}TiO_3$ System. *Sci. Rep.* **2016**, *6*, No. 33392.

(20) Keswani, B. C.; Devan, R. S.; Kambale, R. C.; James, A. R.; Manandhar, S.; Kolekar, Y. D.; Ramana, C. V. Correlation between structural, magnetic and ferroelectric properties of Fe-doped (Ba-Ca)TiO_3 lead-free piezoelectric. *J. Alloys Compd.* **2017**, *712*, 320−333.

(21) Jian, G.; Jiao, Y.; Meng, Q.; Shao, H.; Wang, F.; Wei, Z. 3D $BaTiO_3$ Flower Based Polymer Composites Exhibiting Excellent Piezoelectric Energy Harvesting Properties. *Adv. Mater. Interfaces* **2020**, *7*, 2070089.

(22) Bersuker, I. B.; Polinger, V. Perovskite Crystals: Unique Pseudo-Jahn−Teller Origin of Ferroelectricity, Multiferroicity, Permittivity, Flexoelectricity, and Polar Nanoregions. *Condensed Matter* **2020**, *5*, 68.

(23) Yan, X.; Lam, K. H.; Li, X.; Chen, R.; Ren, W.; Ren, X.; Zhou, Q.; Shung, K. K. Lead-free intravascular ultrasound transducer using BZT-50BCT ceramics. *IEEE Trans. Sonics Ultrason.* **2013**, *60*, 1272−1276.

(24) Chao, X.; Wang, J.; Pu, J.; Zhang, S.; Yang, Z. Aging behavior and electrical properties of low-temperature sintered (Ba, Ca)(Ti, Zr)O_3-Ba(Cu,W)O_3 ceramics and plate loudspeaker. *Sens. Actuators, A* **2016**, *237*, 9−19.
(25) Zhu, X. N.; Zhang, W.; Chen, X. M. Enhanced dielectric and ferroelectric characteristics in Ca-modified $BaTiO_3$ ceramics. *AIP Adv.* **2013**, *3*, 082125.
(26) Keeble, D. S.; Benabdallah, F.; Thomas, P. A.; Maglione, M.; Kreisel, J. Revised structural phase diagram of ($Ba_{0.7}Ca_{0.3}TiO_3$)-($BaZr_{0.2}Ti_{0.8}O_3$). *Appl. Phys. Lett.* **2013**, *102*, 092903.
(27) Mahajan, S.; Thakur, O. P.; Prakash, C.; Sreenivas, K. Effect of Zr on dielectric, ferroelectric and impedance properties of $BaTiO_3$ ceramic. *Bull. Mater. Sci.* **2011**, *34*, 1483−1489.
(28) Yan, H.; Inam, F.; Viola, G.; Ning, H.; Zhang, H.; Jiang, Q.; Zeng, T. A. O.; Gao, Z.; Reece, M. J. The Contribution of Electrical Conductivity, Dielectric Permittivity and Domain Switching in Ferroelectric Hysteresis Loops. *J. Adv. Dielectr.* **2011**, *01*, 107−118.
(29) Zhang, L.; Zhao, L.; He, L.; Wang, D.; Sun, Y.; Wang, D.; Lou, X.; Zhang, L.; Carpenter, M. A. New Degree of Freedom in Determining Superior Piezoelectricity at the Lead-Free Morphotropic Phase Boundary: The Invisible Ferroelectric Crossover. *ACS Appl. Mater. Interfaces* **2022**, *14*, 1434−1442.
(30) Gutierrez, G.; Sundin, E. M.; Nalam, P. G.; Zade, V.; Romero, R.; Nair, A. N.; Sreenivasan, S.; Das, D.; Li, C.; Ramana, C. V. Interfacial Phase Modulation-Induced Structural Distortion, Band Gap Reduction, and Nonlinear Optical Activity in Tin-Incorporated Ga_2O_3. *J. Phys. Chem. C* **2021**, *125*, 20468−20481.
(31) Mallesham, B.; Roy, S.; Bose, S.; Nair, A. N.; Sreenivasan, S.; Shutthanandan, V.; Ramana, C. V. Crystal Chemistry, Band-Gap Red Shift, and Electrocatalytic Activity of Iron-Doped Gallium Oxide Ceramics. *ACS Omega* **2020**, *5*, 104−112.
(32) Keswani, B. C.; Patil, S. I.; James, A. R.; Kolekar, Y. D.; Ramana, C. V. Correlation between structural, ferroelectric, piezoelectric and dielectric properties of $Ba_{0.7}Ca_{0.3}TiO_3$-x$BaTi_{0.8}Zr_{0.2}O_3$ (x = 0.45, 0.55) ceramics. *Ceram. Int.* **2018**, *44*, 20921−20928.
(33) Kalidindi, N. R.; Manciu, F. S.; Ramana, C. V. Crystal structure, phase, and electrical conductivity of nanocrystalline $W_{(0).(9)(5)}Ti_{((0).(0)(5))}O_{(3)}$ thin films. *ACS Appl. Mater. Interfaces* **2011**, *3*, 863−868.
(34) Ramana, C. V.; Ait-Salah, A.; Utsunomiya, S.; Morhange, J. F.; Mauger, A.; Gendron, F.; Julien, C. M. Spectroscopic and Chemical Imaging Analysis of Lithium Iron Triphosphate. *J. Phys. Chem. C* **2007**, *111*, 1049−1054.
(35) Pinczuk, A.; Taylor, W.; Burstein, E.; Lefkowitz, I. The Raman spectrum of $BaTiO_3$. *Solid State Commun.* **1967**, *5*, 429−433.
(36) Nafie, L. A., *Encyclopedia of Spectroscopy and Spectrometry (Third Edition)*; Academic Press, 2017, pp 891−899.
(37) Mu, X.; Chen, X.; Wang, J.; Sun, M. Visualizations of Electric and Magnetic Interactions in Electronic Circular Dichroism and Raman Optical Activity. *J. Phys. Chem. A* **2019**, *123*, 8071−8081.
(38) Venkateswaran, U. D.; Naik, V. M.; Naik, R. High-pressure Raman studies of polycrystalline $BaTiO_3$. *Phys. Rev. B* **1998**, *58*, 14256−14260.
(39) DiDomenico, M.; Wemple, S. H.; Porto, S. P. S.; Bauman, R. P. Raman Spectrum of Single-Domain $BaTiO_3$. *Phys. Rev.* **1968**, *174*, 522−530.
(40) Cao, S.; Xu, J.; Jin, L.; Zhao, J.; Ma, Z.; Chen, Q.; Liu, J.; Gao, F. Microstructure and bidirectional dielectric tunability behaviour of Nd^{3+}-doped $KSr_2Nb_5O_{15}$ lead-free ceramics. *J. Materiomics* **2021**, *7*, 976−987.
(41) Bouaamlat, H.; Hadi, N.; Belghiti, N.; Sadki, H.; Naciri Bennani, M.; Abdi, F.; Lamcharfi, T.-d.; Bouachrine, M.; Abarkan, M. Dielectric Properties, AC Conductivity, and Electric Modulus Analysis of Bulk Ethylcarbazole-Terphenyl. *Adv. Mater. Sci. Eng.* **2020**, *2020*, 1−8.
(42) Keswani, B. C.; Patil, S. I.; James, A. R.; Nath, R. C.; Boomishankar, R.; Kolekar, Y. D.; Ramana, C. V. Structural, magnetic and ferroelectric properties of lead free piezoelectric 0.9-(0.45$Ba_{0.7}Ca_{0.3}TiO_3$−0.55$BaTi_{0.8}Zr_{0.2}O_3$) and magnetostrictive 0.1-($Co_{0.7}Mn_{0.3}Fe_{1.95}Dy_{0.05}O_4$) magnetoelectric particulate composite. *J. Appl. Phys.* **2019**, *126*, 224101.
(43) Dorey, R. A. *Ceramic Thick Films for MEMS and Microdevices Ebook*, William Andrew, 2011.
(44) Roth, W. A. Landolt-Börnstein Physikalisch-chemische Tabellen. *Nature* **1937**, *139* (3507), 93−93.
(45) Wang, X.; Zhang, L.; Liu, H.; Zhai, J.; Yao, X. Dielectric nonlinear properties of $BaTiO_3$−$CaTiO_3$−$SrTiO_3$ ceramics near the solubility limit. *Mater. Chem. Phys.* **2008**, *112*, 675−678.
(46) Liu, G.; Zhang, S.; Jiang, W.; Cao, W. Losses in Ferroelectric Materials. *Mater. Sci. Eng. R Rep.* **2015**, *89*, 1−48.
(47) Sharma, A. P.; Pradhan, D. K.; Pradhan, S. K.; Bahoura, M. Large energy storage density performance of epitaxial BCT/BZT heterostructures via interface engineering. *Sci. Rep.* **2019**, *9*, No. 16809.
(48) Chen, C.; Zhuang, H.; Zhu, X.; Zhang, D.; Zhou, K.; Yan, H. Effect of Ca substitution sites on dielectric properties and relaxor behavior of Ca doped barium strontium titanate ceramics. *J. Mater. Sci.: Mater. Electron.* **2015**, *26*, 2486−2492.
(49) Viola, G.; Saunders, T.; Wei, X.; Chong, K. B.; Luo, H.; Reece, M. J.; Yan, H. Contribution of piezoelectric effect, electrostriction and ferroelectric/ferroelastic switching to strain-electric field response of dielectrics. *J. Adv. Dielectr.* **2013**, *03*, 1350007.
(50) Baraskar, B. G.; Kadhane, P. S.; Darvade, T. C.; James, A. R.; Kambale, R. C. BaTiO3-Based Lead-Free Electroceramics with Their Ferroelectric and Piezoelectric Properties Tuned by Ca^{2+}, Sn^{4+} and Zr^{4+} Substitution Useful for Electrostrictive Device Application. In *Ferroelectrics and Their Applications*, 2018.
(51) Wu, J. Perovskite lead-free piezoelectric ceramics. *J. Appl. Phys.* **2020**, *127*, 190901.
(52) Praveen, J. P.; Kumar, K.; James, A. R.; Karthik, T.; Asthana, S.; Das, D. Large piezoelectric strain observed in sol−gel derived BZT−BCT ceramics. *Curr. Appl. Phys.* **2014**, *14*, 396−402.
(53) Lupascu, D. C. *Fatigue in Ferroelectric Ceramics and Related Issues*, Springer Science & Business Media, 2004.
(54) Mezheritsky, A. V. Quality Factor of Piezoceramics. *Ferroelectrics* **2002**, *266*, 277−304.
(55) Pertsev, N. A.; Dkhil, B. Strain sensitivity of polarization in perovskite ferroelectrics. *Appl. Phys. Lett.* **2008**, *93*, 122903.
(56) M. Nor, N., Hamzah, H. H., Abdul Razak, K. Recent Advancement in Sustainable Energy Harvesting Using Piezoelectric Materials. In *Sustainable Materials for Next Generation Energy Devices*, Cheong, K. Y., Chen, L.-C., Eds.; Elsevier, 2021; pp 221−248.
(57) Uchino, K. The Development of Piezoelectric Materials and the New Perspective. In *Advanced Piezoelectric Materials*, Uchino, K., Ed.; Woodhead Publishing, 2010; pp 1−85.
(58) Takenaka, T. Lead-Free Piezoelectric Ceramics. In *Handbook of Advanced Ceramics*, 2nd ed., Somiya, S., Ed.; Academic Press: Oxford, 2013; Chapter 6.2, pp 429−446.
(59) Potong, R.; Rianyoi, R.; Ngamjarurojana, A.; Chaipanich, A. Dielectric and piezoelectric properties of 1−3 non-lead barium zirconate titanate-Portland cement composites. *Ceram. Int.* **2013**, *39*, S53−S57.
(60) Sharma, P.; Kumar, P.; Kundu, R. S.; Ahlawat, N.; Punia, R. Enhancement in magnetic, piezoelectric and ferroelectric properties on substitution of titanium by iron in barium calcium titanate ceramics. *Ceram. Int.* **2016**, *42*, 12167−12171.
(61) Brajesh, K.; Tanwar, K.; Abebe, M.; Ranjan, R. Relaxor ferroelectricity and electric-field-driven structural transformation in the giant lead-free piezoelectric(Ba,Ca)(Ti,Zr)O_3. *Phys. Rev. B* **2015**, *92*, 224112.
(62) Roy, S.; Maharana, R.; Reddy, S. R.; Singh, S.; Kumar, P.; Karthik, T.; Asthana, S.; Prasad, V. V. B.; Kamat, S. V. Structural, ferroelectric and piezoelectric properties of chemically processed, low temperature sintered piezoelectric BZT−BCT ceramics. *Mater. Res. Express* **2016**, *3*, No. 035702.
(63) Hamdi, O.; Mighri, F.; Rodrigue, D. Piezoelectric cellular polymer films: Fabrication, properties and applications. *AIMS Mater. Sci.* **2018**, *5*, 845−869.

https://doi.org/10.1021/acs.cgd.2c00679
Cryst. Growth Des. 2022, 22, 5571−5581